REVIEW

Signal-to-noise ratio of Raman signal measured by multichannel detectors*

Xue-Lu Liu(刘雪璐)[1], Yu-Chen Leng(冷宇辰)[1,2], Miao-Ling Lin(林妙玲)[1], Xin Cong(从鑫)[1,2], and Ping-Heng Tan(谭平恒)[1,2,†]

[1] State Key Laboratory of Superlattices and Microstructures, Institute of Semiconductors, Chinese Academy of Sciences, Beijing 100083, China
[2] Center of Materials Science and Optoelectronics Engineering & CAS Center of Excellence in Topological Quantum Computation, University of Chinese Academy of Sciences, Beijing 100049, China

(Received 8 June 2021; revised manuscript received 1 August 2021; accepted manuscript online 19 August 2021)

Raman spectroscopy has been widely used to characterize the physical properties of two-dimensional materials (2DMs). The signal-to-noise ratio (SNR or S/N ratio) of Raman signal usually serves as an important indicator to evaluate the instrumental performance rather than Raman intensity itself. Multichannel detectors with outstanding sensitivity, rapid acquisition speed and low noise level have been widely equipped in Raman instruments for the measurement of Raman signal. In this mini-review, we first introduce the recent advances of Raman spectroscopy of 2DMs. Then we take the most commonly used CCD detector and IGA array detector as examples to overview the various noise sources in Raman measurements and analyze their potential influences on SNR of Raman signal in experiments. This overview can contribute to a better understanding on the SNR of Raman signal and the performance of multichannel detector for numerous researchers and instrumental design for industry, as well as offer practical strategies for improving spectral quality in routine measurement.

Keywords: multichannel detectors, signal-to-noise ratio, dark noise, shot noise

PACS: 78.30.−j, 43.50.Yw, 85.60.Gz, 43.60.Cg **DOI:** 10.1088/1674-1056/ac1f06

1. Introduction

The successful exfoliation of the first true two-dimensional structure, monolayer graphene,[1] stimulates intense interest in two-dimensional materials (2DMs).[2,3] In 2DMs, the atoms within each layer are joined together by covalent bonds, while adjacent layers in 2DMs are weakly coupled to each other and can be easily exfoliated and isolated down to monolayer and few layers. The quantum confinement in atomic scale and the presence of interlayer coupling in multilayer 2DMs make their electronic and optical properties varying with layer number.[4] Plenty of spectroscopic techniques[5–9] have been used to characterized these novel properties of 2DMs. Among them, Raman spectroscopy, one of the most important nondestructive, fast and relatively inexpensive characterization tools, can provide abundant structural and electronic information with high spatial resolution at both laboratory and mass-production scales, which has been widely used to characterize layer numbers, interlayer coupling and layer-stacking configurations of 2DMs.[10–13]

In general, Raman spectra of 2DMs can be classified into two types, intralayer and interlayer modes, which mainly stem from the intralayer chemical bonds and interlayer van der Waals (vdW) forces, respectively. The investigations on intralayer modes of 2DMs were firstly performed in few layer graphene, providing useful information on the defects as well as the stacking order. Three optical modes dominate the intralayer modes of graphene, i.e., G mode, D mode and 2D mode. The G mode is associated with the doubly degenerate longitudinal optical (LO) and in-plane transverse optical (TO) phonon (E_{2g} symmetry) at the Brillouin zone (BZ) center and is a characteristic peak of graphene-related materials. While the D mode comes from TO phonons around the Brillouin zone edge near K point and requires a defect for activation.[13] The 2D mode arises from the overtone of TO phonons around the K point and is activated by triple resonance Raman scattering. Ferrari *et al.*[14] have successfully explained the physical origins for the changes of the 2D modes in shape, linewidth and peak position for graphene layers. Then Zhao *et al.*[15] demonstrated that the changes of the 2D modes can be used to identify the layer numbers of few layer graphene with AB stacking once the excitation wavelength is 633 nm. Moreover, the line shape of the 2D modes was also proved to be dependent on the stacking order of multilayer graphene.[16] In addition, the frequencies of intralayer modes of transition metal dichalcogenides (TMD) also show significant layer-dependent behaviors. For example, in N-layer MoS_2 (NL-MoS_2), with increasing layer number of N, the frequency of the E^1_{2g} mode ($\omega(E^1_{2g})$) decreases and that of the A_{1g} mode ($\omega(A_{1g})$) increases.[17] The oppo-

*Project supported by the National Key Research and Development Program of China (Grant No. 2016YFA0301204), the National Natural Science Foundation of China (Grant No. 11874350), and Key Research Program of the Chinese Academy of Sciences (Grant Nos. XDPB22 and ZDBS-LY-SLH004).

†Corresponding author. E-mail: phtan@semi.ac.cn

site trends of $\omega(E^1_{2g})$ and $\omega(A_{1g})$ with N are attributed to the surface effect,[18] providing a feasible method to identify the layer number. In comparison with the intralayer modes with high frequency, the interlayer modes have very low frequencies, usually below 100 cm^{-1}. Thanks to the improved Raman scattering technique to detect the low frequency region,[19] investigations on interlayer Raman modes recently become increasingly popular.[20] For example, the frequency of interlayer modes now is widely used to identify the layer number of 2DMs and the strength of interlayer coupling.[9,19–22] Raman spectroscopy also shows its great potential in the characterization of van der Waals heterostructures (vdWHs).[23,24] Plenty of exciting physical phenomena have been observed using Raman spectroscopy, such as moiré phonons in twisted TMD flakes[25,26] and cross-dimensional electron–phonon coupling in vdWHs.[27]

Although Raman spectroscopy has shown lots of advantages in the characterization of 2DMs and vdWHs, the efficiency of Raman scattering is extremely low in comparison with other optical processes. Moreover, various noise signals could also be captured by the detector in Raman measurements, which further brings difficulties to spectrum analysis and peak assignment of weak Raman signals. Optimizing detection performance and reducing noise are common desires from scientific instrument companies as well as researchers. Signal-to-noise ratio (SNR or S/N ratio) is a commonly used estimator of a Raman system's ability to extract analytical information of Raman signals from noise signals. The SNR largely depends on the estimation of noise in spectra. But it is still a subject of ongoing debate and confusion to determine the noise level from the experimental Raman spectrum.[28–33] It is of great practical significance to overview the different noise sources and their influences on SNR, and further to experimentally estimate SNR of Raman spectrum taken by multichannel detectors.

The noise level of the detector in Raman instrument is one of the main factors that affect the SNR and is also an important indicator to evaluate the performance of a detector. It is very important to choose a detector with low noise and high sensitivity for Raman measurements. Multichannel detector has high quantum efficiency, which can greatly reduce the time of signal acquisition in comparison with single-channel detector. The widespread popularity of multichannel detectors greatly promotes the application of Raman spectrometer in experimental research and the development of portable Raman spectrometer. For single-channel detector in traditional Raman system, the inhomogeneous current fluctuation would lead to noise level variation in consecutive acquisitions. Therefore, the statistical analysis of SNR should be based on the capture of single datum performed by single-channel detector with multiple acquisitions. In contrast, multichannel detectors used in modern Raman spectrometer generally consist of hundreds to thousands of independent photo-sensors or pixels in one-dimensional direction to collect Raman signals with different wavelengths at the same time, which makes it unrealistic in technology to evaluate the SNR for Raman signal by monitoring each pixel with multiple acquisitions. Because every pixel in multichannel detector is expected to have basically the same quality and performance, it is reasonable to statistically analyze the pixels around the signal peak in one measurement to evaluate the general performance of the multichannel detector due to the high density of data in Raman spectrum. However, multichannel detector can be designed to work at different temperatures with software-selectable gains. Different detectors also exhibit specific non-uniformity and nonlinearity in photoelectric response. For example, the non-uniformity in photoelectric response of InGaAs (IGA) array detector can be up to $\pm$ 10%. Thus, the noise level, photoelectric response and efficiency of different pixels of a charge-coupled-device (CCD) detector and IGA detector can vary in a large range. In this case, in order to obtain the intrinsic noise level of multichannel detector, two or more Raman measurements are necessary to exclude the effect of non-uniformity and nonlinearity between different pixels. As the non-sample noise source has changed from inhomogeneous current fluctuation in single-channel detector to the non-uniformity of pixels in multichannel detector, the noise analysis for SNR estimation has changed accordingly. It is of great practical significance to propose more adaptive SNR evaluation methods based on a few acquisitions of spectra taken by multichannel detector.

In this mini-review, we will firstly address the recent investigations of 2DMs studied by Raman spectroscopy in Section 2, and then overview the importance of SNR in Raman spectroscopy in Section 3. Sections 4 and 5 will introduce different noise sources and experimentally analyze their influences on SNR of Raman signal detected by CCD detectors and IGA array detector. Finally, in Section 6, a generic analytical method is provided to estimate SNR of the measured Raman signals.

2. Recent advances on Raman spectroscopy of two-dimensional materials

Since the 1960s, the introduction of laser light sources, the development of weak signal detection techniques and computer applications have led to the rapid development of Raman spectroscopy technology and made it widely used in scientific and industrial applications to characterize lattice structure and physical properties of materials.[34] In recent years, the unique properties of graphene[35] triggered a huge amount of innovative scientific researches and experiments on 2DMs. As a non-destructive technique, Raman spectroscopy becomes increasingly important in the area of 2DMs. As mentioned before, Raman spectra of 2DMs contain interlayer and intralayer modes. In 2DMs, there are two types of interlayer modes,

i.e., the shear (S) and layer-breathing (LB) modes, which correspond to the relative motions of the atom planes parallel and perpendicular to the basal plane, respectively. In general, several branches of the S and LB modes can be observed in 2DMs.[36] For an N-layer (NL) 2DM, there are $N-1$ pairs of S modes and $N-1$ LB modes, which are denoted as $S_{N,N-j}$ and $LB_{N,N-j}$ ($j=1,2,\ldots,N-1$). Among them, $S_{N,1}$ ($LB_{N,1}$) (i.e., $j=N-1$) is the one with the highest frequency while $S_{N,N-1}$ ($LB_{N,N-1}$) (i.e., $j=1$) is the one with the lowest frequency. The frequencies of the S and LB modes are sensitive to interlayer coupling and can be well described by the linear chain mode (LCM).[19,36,37] Based on LCM, each layer of an NL 2DM can be treated as a single ball so that the 2DM can be simplified as a linear chain with balls in which only nearest-neighbor interlayer interaction is considered. Assuming that the nearest-neighbor force constants per unit area for the S and LB modes are $\alpha_0^{\parallel}$ and $\alpha_0^{\perp}$, respectively, the corresponding dynamic matrix can be built up.[38] By solving the dynamic matrix, the frequencies of the $S_{N,N-j}$ and $LB_{N,N-j}$ modes in the NL 2DMs can be, respectively, expressed by[36]

$$\begin{aligned}\omega(S_{N,N-j}) &= \omega(S_{bulk})\sin(j\pi/2N),\\ \omega(LB_{N,N-j}) &= \omega(LB_{bulk})\sin(j\pi/2N),\end{aligned} \tag{1}$$

where $\omega(S_{bulk})=\frac{1}{\pi c}\sqrt{\alpha_0^{\parallel}/\mu}$ and $\omega(S_{bulk})=\frac{1}{\pi c}\sqrt{\alpha_0^{\perp}/\mu}$, c is the speed of light, and μ is the monolayer mass per unit area. Figure 1(a) shows the branches ($j=N-1,N-2,\ldots$) for the S modes and Fig. 1(b) shows the branches ($j=1,2,\ldots$) for the LB modes. It is found that once $\omega(S_{bulk})$ and $\omega(S_{bulk})$ are normalized to $\sqrt{2}$, the frequencies of the S and LB modes of the bilayer 2DMs are equal to 1, i.e., $\omega(S_{2,1})=\omega(LB_{2,1})=1$. The normalized experimental frequencies[36] of the S (circles) and LB modes (squares) in NL MoS_2 by the corresponding $\omega(S_{2,1})$ and $\omega(LB_{2,1})$ are included Figs. 1(a) and 1(b), respectively. The experimental data can be well modeled by the LCM. The LCM of Eq. (1) describes a robust link between $\omega(S_{N,N-j})$ and $\omega(LB_{N,N-j})$ with N in NL 2DMs, which has been widely utilized as a fast method to identify the flake thickness of multilayer 2DMs.[39,40]

Figure 2(a) shows the typical layer-dependent interlayer modes in 2H-stacked N layer $MoTe_2$ (NLM). Both S and LB modes show significant dependence on the layer number N. The observed S modes come from the branch ($j=N-1$) whose frequency increases with increasing N, while the observed LB modes come from the branches ($j=1,3$) whose frequencies decrease with increasing N. Interlayer modes are also observed experimentally in vdWHs,[41,42] such as twisted multilayer $MoTe_2$ (also denoted as $t(m+n)$LM),[43] as illustrated in Fig. 2(b). More LB modes arise in $t(m+n)$LM due to their low lattice symmetry. For S modes, only the S modes of the mLM and nLM constituents can be observed in Raman spectra, for example, $S_{3,1}$ in t(1+3)LM and t(2+3)LM (Figs. 2(c) and 2(d)). No S mode is observed in t(1+1)LM. The experimental (blue diamonds and red circles) frequencies of interlayer modes in NLM and $t(m+n)$LM are summarized in Figs. 2(c) and 2(d), respectively, showing good agreement with the theoretical (blue and red crosses) results that calculated by LCM. The results indicate that interface twist exhibits a little influence on the LB coupling strength in $t(m+n)$LM, and ω(LB) is only determined by the total layer number N of $t(m+n)$LM ($N=m+n$). While the twisted interface weakens the interfacial shear coupling between the constituents of $t(m+n)$LM so that only the S modes of the mLM and nLM constituents can be observed in Raman spectra. Similar results have been observed in other vdWHs.[44,45] Based on the above discussions, one can conclude that, the total layer number of vdWH and its constituents can be identified according to the observed ω(LB) and ω(C), respectively.

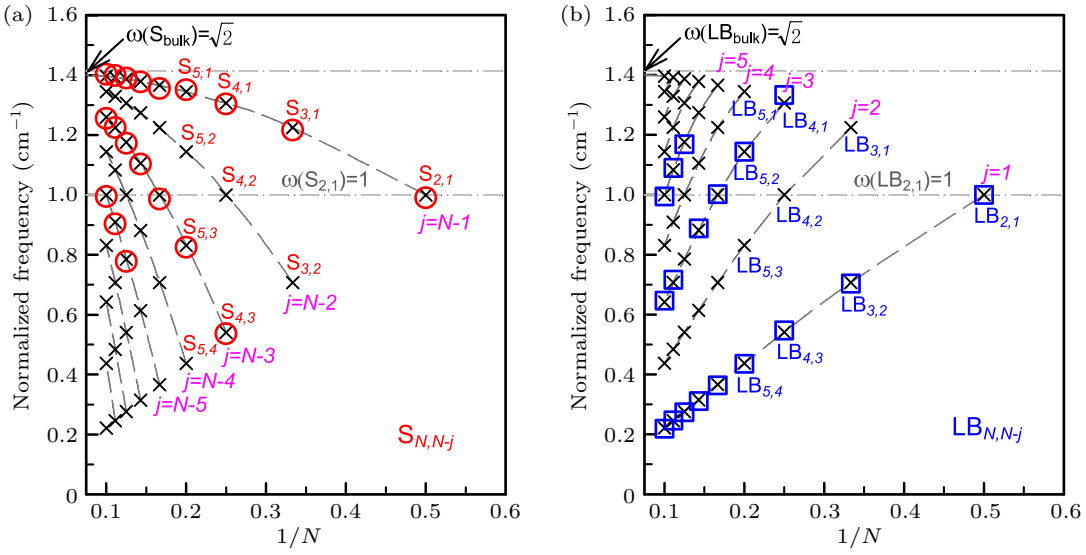

Fig. 1. The frequencies of the interlayer S (a) and LB (b) modes in NL 2DMs as a function of inverse layer number (N), where $\omega(S_{2,1})$ and $\omega(LB_{2,1})$ are normalized to 1. The circles in (a) and squares in (b) are the normalized experimental frequencies[9] of the S and LB modes in NL MoS_2 by the corresponding $\omega(S_{2,1})$ and $\omega(LB_{2,1})$, respectively. Reproduced from Ref. [36]. Copyright 2016, the Royal Society of Chemistry.

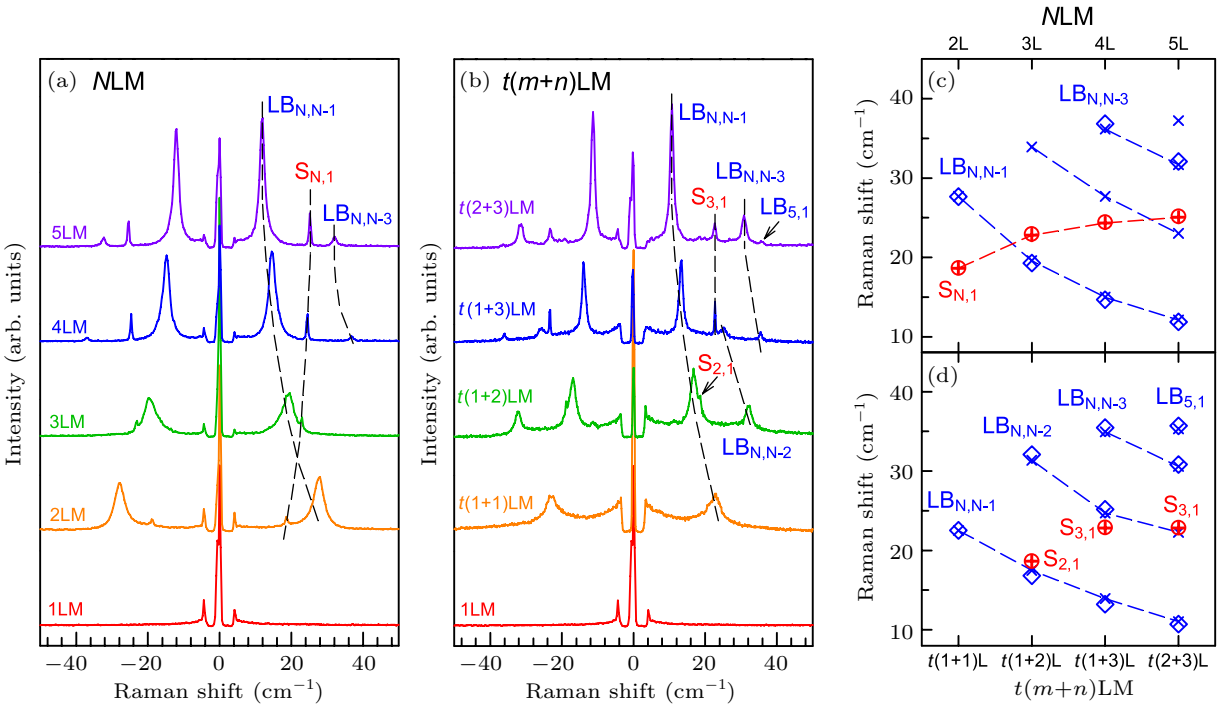

Fig. 2. Raman spectra of interlayer modes in (a) NLM and (b) $t(m+n)$LM. The calculated frequencies of S (red crosses) and LB modes (blue crosses) in (c) 2LM-5LM and the corresponding (d) $t(m+n)$LM based on LCM. The experimental frequencies of the S (red circles) and LB (blue diamonds) modes are also shown.

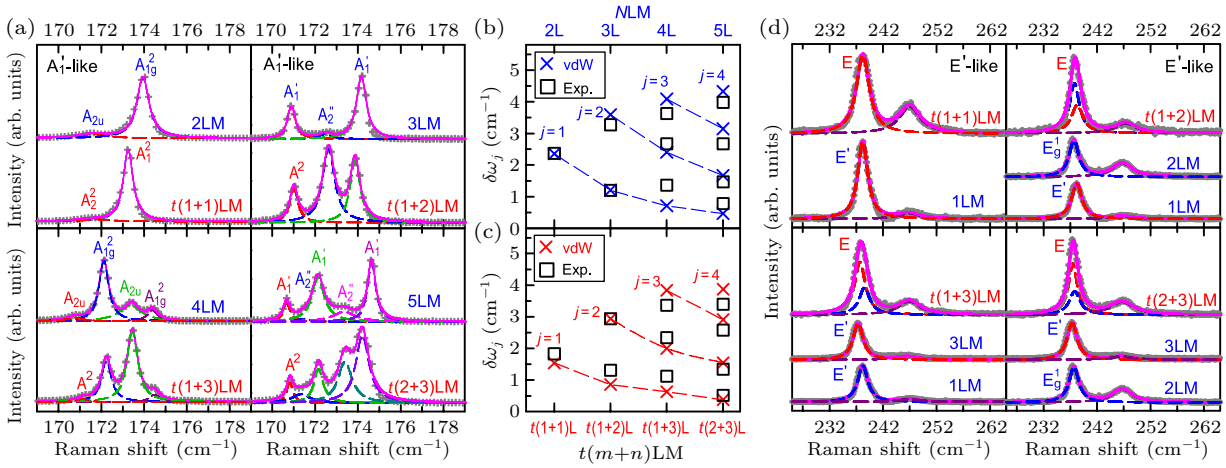

Fig. 3. (a) The Raman spectra of Davydov splitting between Davydov entities of A_1'-like modes of $MoTe_2$ in $t(m+n)$LM and the corresponding NLM ($N=m+n$) at 4 K (gray crosses). The corresponding experimental (black squares) and calculated (crosses) frequency differences between each Davydov entity and the uncoupled one in (b) 2LM-5LM and (c) $t(m+n)$LM. (d) The Raman spectra of E'-like modes in $t(m+n)$LM as well as its constituents mLM and nLM at 4 K (gray crosses) and the fitting results (dashed lines). Reproduced from Ref. [43]. Copyright 2021, the Royal Society of Chemistry.

Intralayer modes with high frequency in NL TMDs also show an N-dependent behavior and have been deeply investigated. In addition to N-dependent frequencies of E_{2g}^1 mode and A_{1g} mode that mentioned before, in NL TMDs, the in-phase (out-of-phase) atomic displacements of the nearest chalcogen atoms between the adjacent layers make the adjacent layers uncoupled (coupled). Thus, each optical mode in 1L TMD splits into a set of N near-degenerate optical modes in NL TMDs, i.e., Davydov splitting.[46–49] Recently, high-resolution resonance Raman spectroscopy at low temperature of 4 K revealed the relation between Davydov splitting of the high-frequency intralayer vibrations and the low-frequency interlayer vibrations.[43]

Figure 3(a) shows the Raman spectra of the out-of-plane intralayer modes in $t(m+n)$LM and the corresponding NLM ($N=m+n$) at 4 K. Due to the complex exciton resonance behavior, all the N Davydov entities of the A_1'-like modes are observed. Notably, the Davydov entities in $t(m+n)$LM exhibit different frequencies from the corresponding entities in NLM. The vdW model,[47] in which the interlayer coupling is considered as a first-order perturbation, is used to understand this phenomenon. We assume the frequency of the uncoupled entity that all the layers are uncoupled as ω_0, i.e., the lowest-frequency entity, whereas the frequency of the j^{th} coupled en-

tity is ω_{cj}. In the case of a first order approximation, the relation of the frequencies of Davydov entities (ω_0 and ω_{cj}) and the j^{th} interlayer mode ($\Delta\omega_j$) is established as follows:

$$\omega_{cj}^2 = \omega_0^2 + (\Delta\omega_j)^2, \tag{2}$$

where $j = 1, 2, \ldots, N-1$. The calculated frequency differences ($\delta\omega_j$) between the coupled entities (ω_{cj}) and uncoupled entity (ω_0) in NLM and $t(m+n)$LM are depicted in Figs. 3(b) and 3(c), respectively. The calculated $\delta\omega_j$ are consistent with the experimental results. Based on the vdW model, the following equation can be easily obtained:

$$\delta\omega_j \approx (\omega(\mathrm{LB}_{N,N-j}))^2/2\omega_0. \tag{3}$$

Because the weaker interfacial coupling at twisted interface results in smaller $\omega(\mathrm{LB}_{N,N-j})$, $\delta\omega_j$ in $t(m+n)$LM are smaller than those in corresponding NLM. In contrast to obvious Davydov splitting in out-of-plane intralayer modes, Davydov entities of the in-plane intralayer mode, E'-like mode, can not be resolved in $t(m+n)$LM and NLM. The spectral profile of the E'-like mode in $t(m+n)$LM can be fitted by those of the corresponding modes in nLM and mLM, as illustrated in Fig. 3(d), suggesting that the in-plane intralayer modes in $t(m+n)$LM are localized within its constituents, similar to the case of the corresponding interlayer S modes. The investigation on Davydov splitting promotes the understanding of the effect of interlayer/interfacial coupling on the in-plane and out-of-plane intralayer modes in pristine and twisted 2DMs.

3. Importance of SNR in Raman spectroscopy

Compared with optical processes such as absorption, photoluminescence and Rayleigh scattering, the efficiency of Raman scattering is extremely low, which makes it quite difficult to detect weak Raman signals in the early years of Raman spectroscopy acquisition. How to design and build a Raman spectroscopy system with high efficiency has always been the goal of scientific instrument companies and researchers. Various noise signals could also be captured by the detector along with weak Raman signals in Raman measurements. The noise signals include photon signals from lasers, samples, optical components and external environment that are not the target of the analyzed Raman signals, such as PL, thermal radiation, stray light as well as ambient photons outside Raman system. These interferences may limit the accuracy of quantitative analysis or even determine whether the Raman feature is valid.

For example, for NLM and $t(m+n)$LM flakes, although all the Davydov entities of out-of-plane intralayer modes can be observed experimentally, some weak Raman modes are difficult to be measured or are easily overwhelmed by the surrounding Raman modes due to the weak electron–phonon coupling,[43] such as the A_{2u} mode of 2LM flakes shown in Fig. 4(a) and A_2'' mode of 5LM shown in Fig. 4(b). In addition, various noise signals, including photoluminescence (PL) in Fig. 4(c), can be an interference to the assignment of Raman features. Therefore, it is important to overview the origin of various types of noises and their potential influences on Raman signals. Especially in the Raman measurement of biological samples, due to limited acquisition time, laser power, and collection efficiency, it is crucial to analyze the noise sources and suppress them effectively before acquisition of Raman spectra.[50] In experiments with lower excitation intensity such as Raman imaging, tip-enhanced Raman spectroscopy, external noises and detector noises add up over longer integration time, which complicates spectral assignment and feature extraction of the valid signal.[31]

Because intensity scale and quantum efficiency may be incomparable in different Raman systems, SNR is always utilized in Raman measurement to evaluate the ability of a Raman system to extract analytical information from noises, instead of Raman signal intensity itself. SNR is also widely used in spectrum acquisition and image processing to indicate spectral quality. Since Raman spectrum contains not only the Raman signal but also baseline associated with various noises, the quantitative estimation of SNR is still a subject of ongoing debate and confusion in different applications.

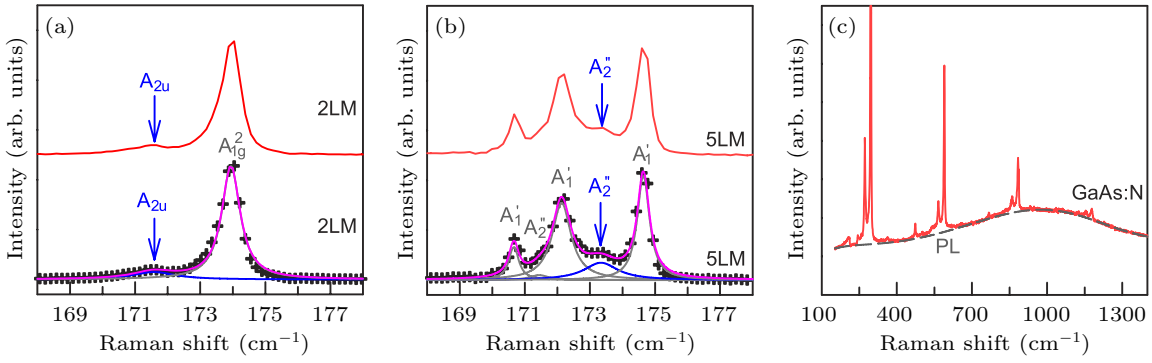

Fig. 4. The Raman spectra of A_1'-like modes in (a) 2LM and (b) 5LM as well as the corresponding fitting results. (a) and (b) are adapted from Ref. [43]. Copyright 2021, the Royal Society of Chemistry. (c) Typical Raman spectra of GaAs:N with a prominent PL background.

The most general definition of SNR is the ratio of the mean peak height above the baseline to the standard deviation of the peak height.[28–31] Another definition of SNR is the peak height above the baseline relative to the baseline noise[32] or the root mean square (RMS) of a flat region of the spectrum.[33] Sometimes signal-to-background ratio (SBR) is used instead, which is defined as the peak height above the baseline relative to baseline amplitude (baseline maximum minus baseline minimum).[32,51] Among these definitions, the key issue is how the noise level is determined from the experimental Raman spectrum, which affects the resulted SNR value accordingly. This may trouble the accurate indication of spectral quality and mislead the performance comparison between different Raman systems.

In the following, we will overview the various noise sources and take the commonly used CCD and IGA detectors as examples to discuss how to evaluate the SNR of Raman signal measured by Raman spectrometer without artificial background substraction and the influence of noise sources on the SNR. Based on this, strategies to improve the SNR ratio of Raman spectroscopy are proposed.

4. Noise analysis of dark spectrum measured by CCD detectors

As illustrated in the introduction, the SNR analysis of a Raman signal is directly related to the standard deviation σ of this Raman signal after multiple measurements by a single-channel detector or a single pixel of multichannel detector. The standard deviation σ is defined as the RMS value of a set of measured values, which describes the mean value of all data's deviations from average and elucidates the degree of dispersion of a data set. Suppose the measured data are $y_1, y_2, \ldots, y_N$, and their average value is $\bar{y}$, then σ can be described as

$$\sigma = \sqrt{\frac{1}{N}\sum_{i=1}^{N}(y_i - \bar{y})^2}. \tag{4}$$

The smaller the σ, the less discrepancy of these values from the average. σ can also be estimated from the fitting to the measured values by the probability density function of Gaussian distribution, i.e.,

$$P(y) = \frac{1}{\sqrt{2\pi}\sigma}\exp\left\{-\frac{(y-\bar{y})^2}{2\sigma^2}\right\}. \tag{5}$$

The probability (or confidence level) of the measured values lying in the confidence interval of $[\bar{y}-\sigma, \bar{y}+\sigma]$ is 68%. A higher confidence level generates a wider confidence interval, for example, 95% and 99.7% confidence levels correspond to confidence intervals of $[\bar{y}-2\sigma, \bar{y}+2\sigma]$ and $[\bar{y}-3\sigma, \bar{y}+3\sigma]$, respectively. This indicates that σ can be roughly estimated by these two confidence intervals from the measured difference spectrum immediately.

In the absence of light, signal detected by detectors is the so-called dark signal, and its corresponding spectrum is known as dark spectrum. The higher the noise in the dark spectrum, the weaker the ability of the spectrometer to detect weak Raman signals. It should be noted that different CCD detectors have their distinct electronic offsets (or electronic bias), which lead to additive offset in the acquired counts or intensity of Raman spectrum.[52] This electronic offset is artificially set to ensure that the analogue-to-digital converter in CCD detector always receives positive signals.[53] Dark noise inherently exists in detectors due to the thermal agitation of electrons in the detector. It is commonly related to the dark signal of the detector that is produced in the absence of light. In principle, both the electronic offset and dark signal are present in a dark spectrum where no light is detected by detector. For LN_2-cooled or TE-cooled CCD detectors working stably below −55 °C,

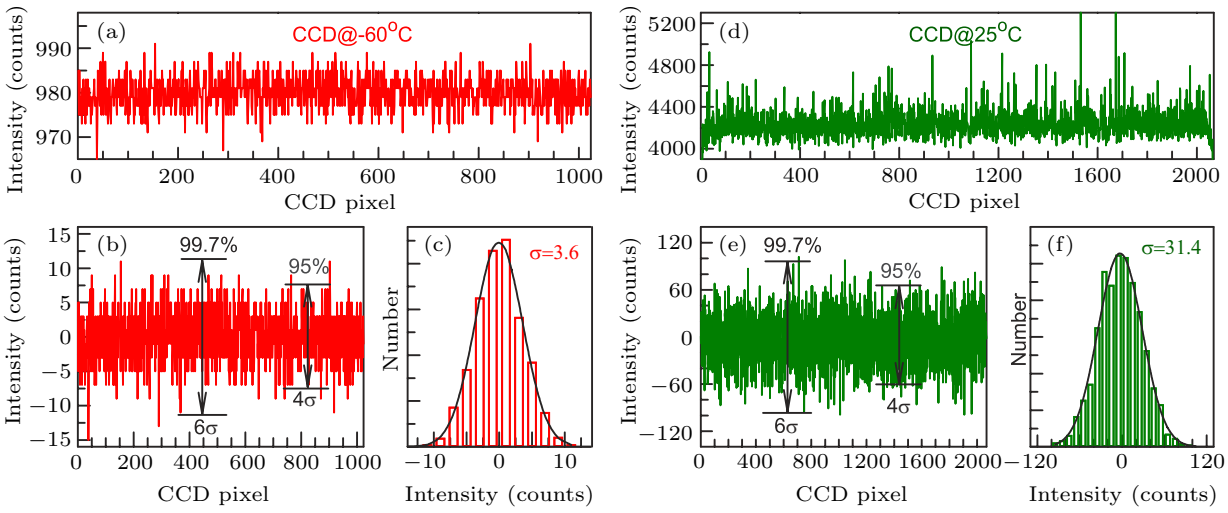

Fig. 5. (a) Typical raw dark spectrum detected by CCD detector working at −60 °C. (b) The spectrum with the electronic offset already deducted from (a). (c) The statistical distribution of the counts of (b) with $\sigma = 3.6$. (d) Typical raw dark spectrum detected by CCD detector working at 25 °C. (e) The difference spectrum of two successive measurements of (d). (f) The statistical distribution of counts of (e) with $\sigma = 31.4$. The acquisition time of (a) and (d) is 1 second.

the dark signal is negligible and only electronic offset ($\sim$ 980 counts in Fig. 5(a)) are present in the dark spectrum. Raman software has an option to simply deduct this additive offset immediately after the spectrum acquisition and directly provides the resulting spectrum without the electronic offset, as shown in Fig. 5(b). Because every pixel of the LN_2-cooled or TE-cooled CCD detectors usually has the same quality and performance, one can statistically analyze σ in the dark spectrum measured by all the CCD pixels in a single acquisition, instead of a single CCD pixel with multiple measurements. As shown in Fig. 5(c), we applied the fitting of the probability density function with Gaussian distribution (Eq. (5)) to the data in Fig. 5(b) and obtained σ of 3.6 for the dark spectrum. This σ indicates the ability of the CCD detector to acquire Raman spectra with high quality. The smaller σ, the better ability of the CCD detector to measure the weak Raman signal emerging from the noise.

The CCD detector working around room temperature exhibits a high level of dark signal. As shown in Fig. 5(d), the inhomogeneity in dark signal of CCD pixels also leads to many distinct spikes, which may hinder the detection of the weak Raman signals. These spikes are consistent during every measurement with the same acquisition time. Thus, we can not get σ by directly analyzing the dark spectrum after the deduction of its electronic offset as the case discussed above for LN_2-cooled or TE-cooled CCD detectors. In this case, to analyze σ for the dark spectrum, these spikes should be excluded by successively obtaining two dark spectra and subtracting one from the other, as shown in Fig. 5(e). In general, such spectrum, obtained by subtracting one spectrum from another one, is known as difference spectrum. Then, σ can be estimated by the Gaussian distribution of the count values from the difference spectrum. The statistical result in Fig. 5(f) gives σ of 31.4, much higher than that in Fig. 5(c), which is expected for the CCD detector working around room temperature. It should be noted that this analysis based on difference spectrum will amplify σ by $\sqrt{2}$ times as will be discussed later.

5. Overview of noise sources in measured Raman spectrum

As discussed in Section 3, the SNR of the measured Raman signal is universally defined as the ratio of its peak height (S) to its standard deviation σ[28–31]

$$\mathrm{SNR} = S/\sigma. \tag{6}$$

The determination of SNR requires the estimation of noise in a spectrum. In principle, σ of the Raman signal mainly comes from the following independent aspects:[28]

σ_S — standard deviation of the Raman signal of interest;

σ_B — standard deviation of the background, including the uninterested Raman signal and the irrelevant photon signals from lasers, samples, and ambient light sources;

σ_d — standard deviation of the dark signal;

σ_F — flicker noise, also known as $1/f$ noise;

σ_r — readout noise.

Among these noise sources, σ_S originates from the intrinsic property of the signal, which is independent of instrument and cannot be eliminated. σ_B, σ_d, σ_F and σ_r are basically instrument-dependent and vary in different devices. Flicker noise is related to the fluctuation in electronic components. It can usually be reduced to a negligible level for multichannel detectors in a well-designed instrument, while a scanning system is very sensitive to the flicker noise depending on the flicker frequency.[28] Therefore, to discuss SNR of Raman signal measured by multichannel detectors, the noise σ is estimated by adding the aforementioned contributions except flicker noise

$$\mathrm{Noise} = \sigma = (\sigma_S^2 + \sigma_B^2 + \sigma_d^2 + \sigma_r^2)^{1/2}. \tag{7}$$

In this section, we will overview the various noise sources of σ based on the analysis in Ref. [28], and further discuss their influences on SNR based on the original Raman spectra measured by CCD detectors and IGA array detector. The following Raman spectra are mainly detected by two typical Raman systems. The home-made *SmartRaman* confocal micro-Raman module (developed by Institute of Semiconductors, Chinese Academy of Sciences) coupled with a Horiba iHR550 spectrometer, and a thermoelectric (TE)-cooled Si CCD detector is utilized for Raman measurement under the 633 nm excitation of a He–Ne laser. This module is also coupled with fiber-optic spectrometer Maya2000 Pro with back-thinned CCD detector working at room temperature. A Horiba HR800 micro-Raman system equipped with a liquid-nitrogen-cooled (LN_2-cooled) linear-array IGA detector and liquid-cooled Si CCD detector is utilized for Raman measurements under 671 nm and 1064 nm excitations.

5.1. Signal shot noise σ_S

Signal shot noise σ_S is caused by the random arrival at the photodiode of the scattered photons, which is a fundamental process to probe Raman signal and exists in all kinds of photodetectors. Due to the particle-like nature of light, the number of photons arriving at the photodiode cannot stay constant all the time, even if the intensity of the scattered light is a constant. Such random fluctuation occurs when counting photons one by one, thus the corresponding noise is called as shot noise. In principle, a discrete random variable of the number of event occurrences is said to have a Poisson distribution, if the events occur with a known constant mean rate and

independent on time. Although the scattered photons arrive at the detector randomly, the number of scattered photons captured by the photodetector per unit time $\dot{S}$ stays constant. Thus, the number of the scattered photons arriving at the photodiode follows the Poisson distribution, in which the probability of a given number of the photons arriving at the photodiode in a fixed time interval of t can be described as

$$P(n) = \frac{(\dot{S}t)^n}{n!}\exp(-\dot{S}t), \tag{8}$$

where $\dot{S}$ is the average number of the counted scattered photons per second, and n is the actual number of scattered photons in t seconds. The shot noise of the Raman signal is equal to the RMS of the number of scattered photons (S) that are captured by detector and contributes to the interested Raman signal, in which $S = \dot{S}t$.

In general, shot noise always exists when counting any physical quantity governed by Poisson statistics. The standard deviation of counts of any random event equals to the square root of the number of events counted. Therefore, the shot noise σ_S equals to the square root of S, i.e., $\sqrt{S} = \sqrt{\dot{S}t}$. When there are few photons, the relative standard deviation σ_S/S can be statistically very large. As the integration time (also referred as exposure time during which the detector is exposed to signals) increases, σ_S increases while σ_S/S decreases. Thus S/σ_S, i.e., $\mathrm{SNR_S}$ of Raman signal, increases.[28]

When the noise from other sources is much smaller than the signal shot noise and can be neglected during the Raman measurements, signal shot noise dominates the noise in Raman signal. Hereinafter we refer this case to as signal shot noise limit, which is possible to occur when the Raman signal is much stronger than the low background. In this case, $\sigma = \sigma_S = \sqrt{S}$, and

$$\mathrm{SNR} = \mathrm{SNR_S} = S/\sigma_S = \dot{S}^{1/2}t^{1/2}. \tag{9}$$

According to Eq. (9), $\mathrm{SNR_S}$ increases with $t^{1/2}$ and thus $\mathrm{SNR_S}$ can be significantly improved by extending the integration time. As shown in Fig. 6, as the integration time is extended from 1 second, 10 seconds to 100 seconds, the background of the spectrum becomes smoother relative to its Raman signal and presents improvement in SNR. However, even for a perfect spectrometer, the SNR will not exceed $\dot{S}^{1/2}t^{1/2}$, which restricts the maximum of SNR to be $\sqrt{S}$.

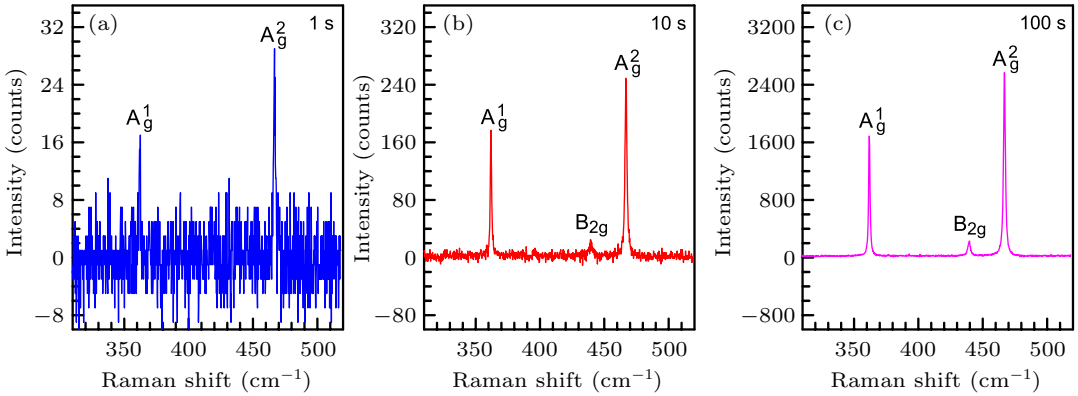

Fig. 6. Raman spectra of black phosphorous excited by 633 nm with different acquisition time: (a) 1 second, (b) 10 seconds, (c) 100 seconds.

5.2. Background shot noise σ_B

"Background" here means any detected photons arising from the laser, sample and surrounding environment other than Raman photons from the analyte at the frequency of interest. Background can come from the Raman instrument, which mainly includes stray light such as laser and plasma, Rayleigh scattering light, non-Raman signals (such as photoluminescence) and uninterested Raman signals from the measured sample, as well as those generated from optical components due to the laser excitation, etc. Also Raman signals of the solvent or impurity and fluorescence from free fluorescent molecules will become the background noise in the obtained surface-enhanced Raman spectrum.[54] These contributions to background are generally sensitive to the change of the laser power. Also, background can also be contributed from stray light not originating in the laser or sample, such as room light, cosmic radiation and other ambient signals, which is generally not sensitive to the laser power.

Background noise is also dominated by shot noise, i.e., background shot noise, which is marked as σ_B.[28] According to the characteristics of shot noise,

$$\sigma_B = B^{1/2} = (\dot{B}t)^{1/2}, \tag{10}$$

where B and $\dot{B}$ denote the intensity statistics of the background signal detected by the detector in time t and per unit time, respectively. Thus, the higher the spectral background, the larger the background shot noise. This can be demonstrated by the cases of Raman spectra of diamond with weak background (Fig. 7(a)) and strong background (Fig. 7(b)). In difference spectrum, the contributions of the Raman signal and

background are removed, and the corresponding background shot noise at positions away from Raman peaks and signal shot noise at positions of Raman peaks can be clearly recognized in Figs. 7(c) and 7(d). The low background counts in Fig. 7(a) result in small σ_B as shown in Fig. 7(c). However, when strong background is superimposed on the Raman peak in Fig. 7(b), background shot noise shown in Fig. 7(d) submerges the signal shot noise even the interested Raman signal in Fig. 7(b) shows the same intensity as that in Fig. 7(a). Since σ_B can be obtained from standard deviation of the corresponding difference spectrum after being divided by $\sqrt{2}$, the spectrum with a near-zero baseline in Fig. 7(c) gives $\sigma_B = 3.9$. While the spectrum with strong background in Fig. 7(d) has a much larger $\sigma_B = 53.3$, demonstrating that the ability to extract Raman features in Fig. 7(d) is largely reduced in the existence of prominent background, even if the Raman signal intensity is the same.

When the noise is dominated by background shot noise, the SNR can be expressed by

$$\mathrm{SNR_B} = S/\sigma_B = \frac{\dot{S}}{\sqrt{\dot{B}}} t^{1/2}. \tag{11}$$

Based on Eq. (11), one can increase SNR by a longer acquisition time, even background may be very strong. Figure 8(a) shows Raman spectrum of a MoS_2 flake deposited on SiO_2/Si substrate. The broad and relatively weak Raman feature of the MoS_2 flake in the range of 350–500 cm^{-1} is almost overwhelmed by strong photoluminescence signal from the MoS_2 flake itself. When the acquisition time is extended, the SNR improves in the manner of $t^{1/2}$. As a result of higher SNR, Raman features of the MoS_2 flake also become prominent despite the rising background, which are illustrated in Figs. 8(b) and 8(c).

The noise from strong background can overwhelm the signal for short integration time. To minimize background shot noise from strong fluorescence is a major motivation for using the lasers in near-infrared or deep-ultraviolet range, especially for biological specimens and semiconductor materials. Background from room light can be partially eliminated by turning off ambient light sources, but such operation may cause inconvenience in daily maintenance, such as optical alignment and calibration. Therefore, in order to obtain high quality Raman signal with high SNR in the routine measurements, it is a key aspect in the design of Raman instruments to eliminate noise contributions from room light.

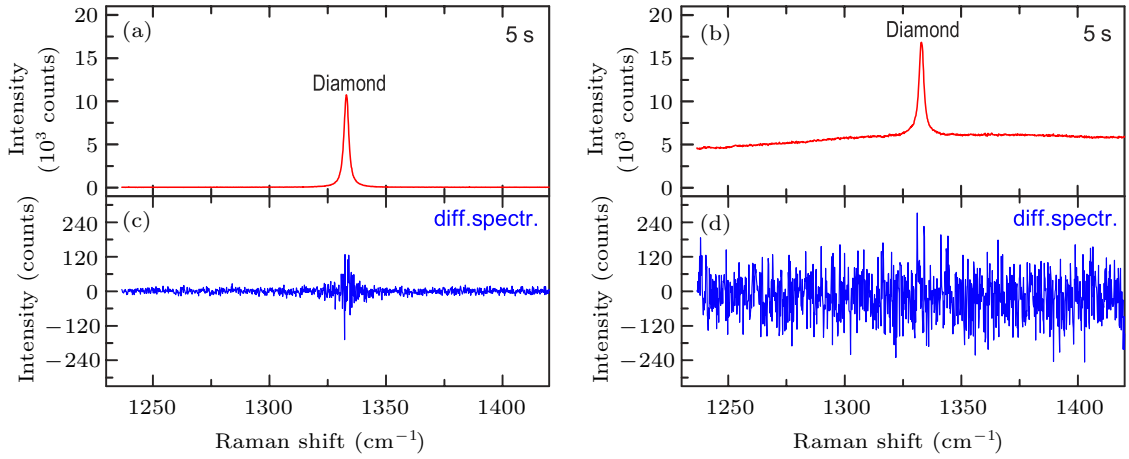

Fig. 7. Raman spectra of diamond with (a) weak background and (b) strong background. (c) The corresponding difference spectrum (diff.spectr.) between two successive measurements of (a). (d) The corresponding diff.spectr. of (b). The acquisition time is 5 seconds.

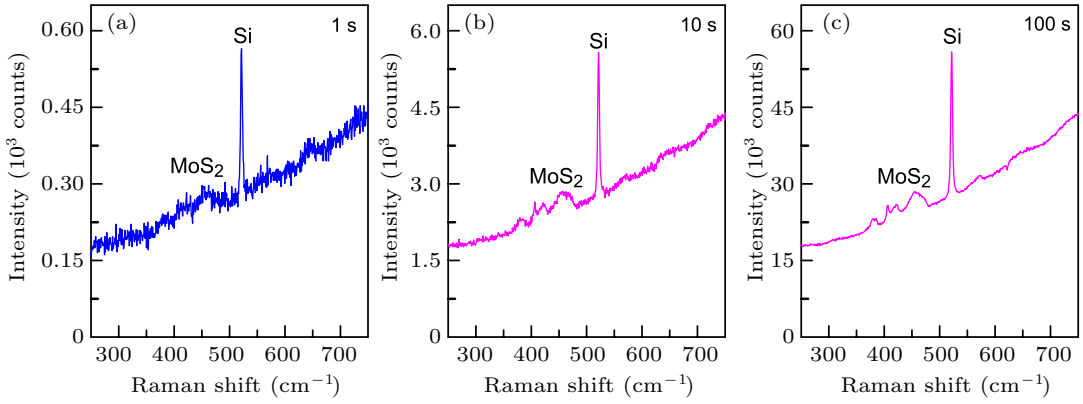

Fig. 8. Raman spectra of a MoS_2 flake on SiO_2/Si substrate excited by 633 nm with integration time of (a) 1 second, (b) 10 seconds and (c) 100 seconds. The strong background comes from photoluminescence of A exciton in MoS_2.

5.3. Detector dark noise σ_d

All detectors currently used in Raman instruments have a finite dark signal, mainly caused by thermal generation of electrons from a photomultiplier cathode or within a solid-state detector.[28] Dark signal directly relates to the acquisition time, which would produce additive quantity to the signal and contribute to the noise level in the measured spectrum. For a given experiment, the contribution of dark signal to the total signal is $\Phi_d t$, where Φ_d is the dark count rate in units of electrons per second ($e^{-1}\cdot s^{-1}$) to illustrate the spontaneous generation rate of electrons in the detector. Φ_d strongly depends on temperature and increases with rising temperature, thus it is usually necessary to cool the detector to reduce the dark signal as illustrated in Figs. 5(a) and 5(d). Φ_d spans in a broad range, from a negligible value ($< 0.001\ e^{-1}\cdot s^{-1}$) in LN_2-cooled CCD detector to a large value ($> 100\ e^{-1}\cdot s^{-1}$) in uncooled detector or near-infrared detector.[28]

As "dark" electrons are counted in the same way as signal or background, the noise of dark signal (also referred to as dark noise) also follows the Poisson statistical distribution as[55]

$$\sigma_d = (\Phi_d t)^{1/2}. \tag{12}$$

Dark noise limit happens when $\Phi_d t$ of the detector (e.g., uncooled detector or near-infrared detector) is much greater than other noises. In this case, the corresponding SNR of Raman signal is

$$\mathrm{SNR}_d = S/\sigma_d = \frac{\dot{S}}{\sqrt{\Phi_d}} t^{1/2}. \tag{13}$$

The dark signal contributes to the detected signal, but it does not depend on the laser power or sample variables. CCD detector working around room temperature and InGaAs array detector usually exhibit high Φ_d and non-uniformity in noise level and photoelectric response between different pixels. The spectrum measured by a detector with high Φ_d has a high-level baseline along with electronic offset. Non-uniformity in dark signal also leads to significant irregular spikes in spectrum apart from Raman and PL signals. Here, we denote the Raman spectrum directly measured by the detector without any processing as raw Raman spectrum, in which the background signals and other stray photon signals are involved, and the Raman spectrum minus the CCD dark spectrum as dark-subtracted Raman spectrum. As shown in Figs. 9(a) and 9(c), irregular spikes caused by non-uniform dark signals can overwhelm intrinsic Raman signal in the raw spectrum. In this case, one needs to measure a dark spectrum with the same acquisition time as the raw spectrum by closing the detector shutter or blocking laser incidence on the sample. After subtracting the dark spectrum from the raw spectrum, the resulting dark-subtracted spectrum shows intrinsic Raman signal from the sample with better spectral quality and higher SNR, as presented in Figs. 9(b) and 9(d).

It is instructive to note that the Raman signal of interest is efficiently detected only by part pixels in CCD detector. Non-illuminated section of the CCD area would contribute dark noise and background shot noise to the measured Raman signal. In the Raman experiment, one can set a reduced CCD area by Raman software to exclude the noise contribution from the unused area.

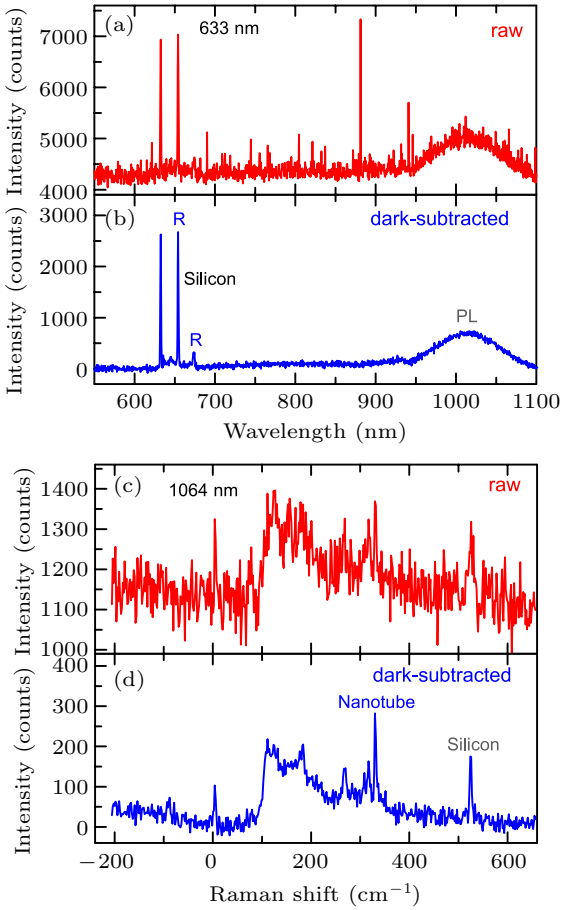

Fig. 9. (a) Raw Raman spectrum of silicon under 633 nm excitation measured by fiber optic spectrometer with a back-thinned CCD detector working at room temperature and (b) the corresponding dark-subtracted spectrum. (c) Raw Raman spectrum of carbon nanotubes deposited on silicon substrate under 1064 nm excitation measured by confocal Raman spectrometer with a LN_2-cooled InGaAs detector and (d) the corresponding dark-subtracted spectrum. Raman signals are marked as R while photoluminescence signals are marked as PL.

5.4. Readout noise σ_r

Readout refers to the process of converting electrons from the detector to a useful form, usually a digital value stored in a computer. Readout noise σ_r is the standard deviation of a large number of readouts from a constant detector signal.[28] For a common CCD detector, the readout noise originates from the transfer process from the stored electrons in the detector into intensity counts through analog-to-digital conversion, whose contribution mainly comes from the amplifier between

the CCD detector and the analog-to-digital converter as well as Johnson (thermal) noise from electronic components. σ_r is strongly related to the type of detector, which may span from a few electrons in a scientific CCD detector to thousands of electrons in a photodiode array. Specific value of σ_r is given in manufacturer's specification. Compared with the dark current of a scientific CCD detector being as low as 0.3 e^-/pixel/h, σ_r cannot be negligible. σ_r is rarely dominant in scientific Raman spectrometer nowadays, except for the detection of rather weak signals or short integration time.[56] In readout noise limit, the SNR of Raman signal is

$$\mathrm{SNR}_r = \frac{\dot{S}}{\sigma_r} t. \tag{14}$$

If Raman signal is not too weak, the effect of σ_r can be eliminated by increasing the integration time.

Readout noise can be regarded as a one-time added type of noise at each pixel for each measurement, thus σ_r does not depend on the signal amplitude nor acquisition time.[28,56] The dark noise and readout noise usually coexist during measurement. Since σ_d is proportional to the integration time while σ_r not, the readout noise can be quantitatively distinguished from dark noise by multiple measurements with different integration time when laser is turned off and background noise is eliminated as much as possible.

Accumulation is often used to obtain a better SNR by repeatedly collecting spectrum and averaging the results. However, when readout noise is dominant, SNR cannot be improved by only increasing the accumulation time. For example, in Fig. 10(a), Raman signal of black phosphorus (BP) is too weak to be detected, completely overwhelmed by readout and dark noises. In this case, it is necessary to increase integration time to improve SNR and make Raman signal more prominent as illustrated in Fig. 10(b). Even though the Raman signal is as low as 2 counts per second, the peak can be clearly discerned from noise after an integration time of 100 seconds. As a comparison, the Raman spectrum with 1 second of integration under 100 times of accumulation in Fig. 10(c) shows much worse SNR even with the same total measurement time as that in Fig. 10(b). Multiple accumulation cannot efficiently improve SNR in readout noise limit because readout noise will pile up with increasing the accumulation number.

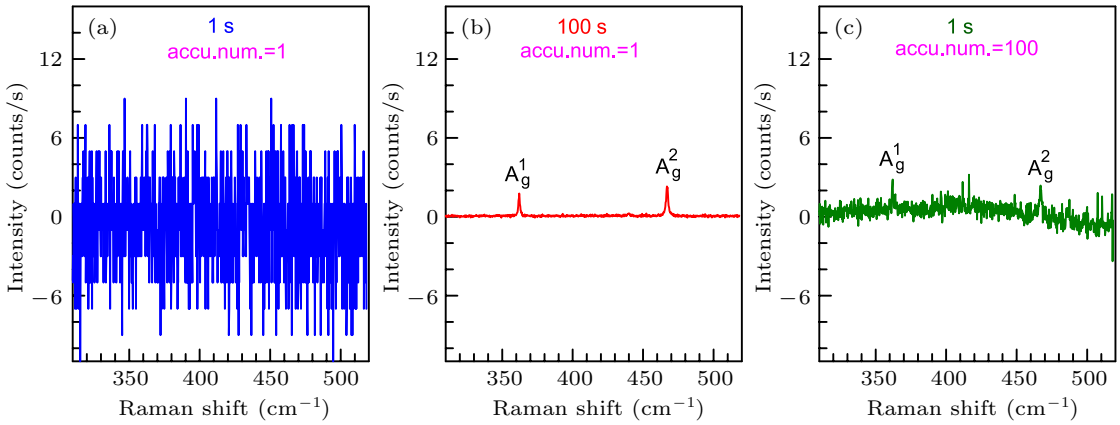

Fig. 10. Raman spectra of BP with integration time of (a) 1 second, (b) 100 seconds, (c) 1 second. The corresponding accumulation number (accu.num.) in (a), (b) and (c) are 1, 1 and 100, respectively. The Raman intensity is in units of counts/s for direct comparison.

6. SNR estimation for the measured Raman signal

If we define the signal as that from the Raman band of interest, the SNR is defined by

$$\mathrm{SNR} = S/(\sigma_S^2 + \sigma_B^2 + \sigma_d^2 + \sigma_r^2)^{1/2}, \tag{15}$$

where S is often defined as the signal due to the Raman feature above a baseline interpolated between spectral regions on either side of the Raman band measured by multichannel detector with low Φ_d and uniform noise level for all pixels. S may be defined either as peak height or peak area above baseline, and the corresponding noise is defined as σ_S.[28] In principle, it is unrealistic for the user to separately measure the noise level generated by each part, but σ_B, σ_d and σ_r can contribute to the noise of baseline, which can be defined as σ_{BL}, i.e., $\sigma_{BL}^2 = \sigma_B^2 + \sigma_d^2 + \sigma_r^2$. In this case, the SNR is defined again by

$$\mathrm{SNR} = S/(\sigma_S^2 + \sigma_{BL}^2)^{1/2}. \tag{16}$$

For the measured Raman signal, if S is taken as Raman peak height I_{Ram} above the baseline, the corresponding $\sigma_S = \sqrt{I_{Ram}}$. For multichannel detectors with low Φ_d and uniform noise level and photoelectric response between different pixels, if the electronic offset is set to zero by Raman software before measurement, the count of the baseline (I_{BL}) at Raman signal of interest is closely associated with σ_{BL}, and the corresponding $\sigma_{BL} = \sqrt{I_{BL}}$. Therefore, the SNR of Raman signal can be practically specified as

$$\mathrm{SNR} \approx I_{Ram}/\sqrt{I_{Ram} + I_{BL}} = I_{Ram}/\sqrt{I_{tot}}, \tag{17}$$

where $I_{\rm tot} = I_{\rm Ram} + I_{\rm BL}$ is the total counts including Raman signal and baseline.

We take the Raman spectrum of GaAsN alloy as an illustration to use Eqs. (16) and (17) for SNR estimation. $GaAs_{1-x}N_x$ with $x = 0.62\%$ is grown by gas-source molecular beam epitaxy on semi-insulating (001) GaAs substrate and a diode pumped solid-state laser at 671 nm is used for resonant excitation of E_+ transition in GaAsN alloy.[57] The Raman spectrum is taken by a liquid-cooled Si CCD detector. Figure 11(a) shows its dark spectrum with $\sigma = 4.2$, whose electronic offset was set to zero by Raman software before measurement. The raw Raman spectrum of GaAsN alloy in Fig. 11(b) shows distinct Raman peaks of GaAs-like longitudinal-optical (LO) zone-center phonon LO(Γ) at 293 cm^{-1} and transverse-optical (TO) zone-center phonon TO(Γ) at 263 cm^{-1}, along with a prominent PL signal as background.[57] We take the Raman peak of the LO(Γ) phonon as a demonstration for typical SNR analysis. As shown in Fig. 11(c), the corresponding $I_{\rm Ram} = 7652$ and $I_{\rm BL} = 11750$ are determined by peak fitting. According to Eq. (17), SNR $= I_{\rm Ram}/\sqrt{I_{\rm tot}} = 7652/\sqrt{7652+11750} = 54.9$. Figure 11(d) shows the difference spectrum between two successive Raman spectra in Fig. 11(b). The difference spectrum can be used to roughly estimate the noise of the baseline in the interested region, i.e., $\sigma_{\rm BL}$, which is equal to the corresponding standard deviation (Fig. 11(d)) divided by $\sqrt{2}$. Figure 11(e) gives $\sigma = 165$, leading to $\sigma_{\rm BL} = 116.7$. Then SNR obtained by Eq. (6) (also Eq. (16)) is SNR $= S/\sigma = S/(\sigma_{\rm S}^2 + \sigma_{\rm BL}^2)^{1/2} = 7652/\sqrt{7652+116.7^2} = 52.5$, which is in agreement with that (54.9) estimated by Eq. (17). The above discussion shows that both Eqs. (16) and (17) can be used to quantify SNR of the measured Raman signal, especially in the limit of signal shot noise, dark noise or background shot noise, i.e., when the Poisson-distributed noise governs the noise level. It should be noted that in the analysis of SNR by Eqs. (16) and (17), electronic offset should be set to zero by Raman software before measurement, otherwise, SNR would be underestimated.

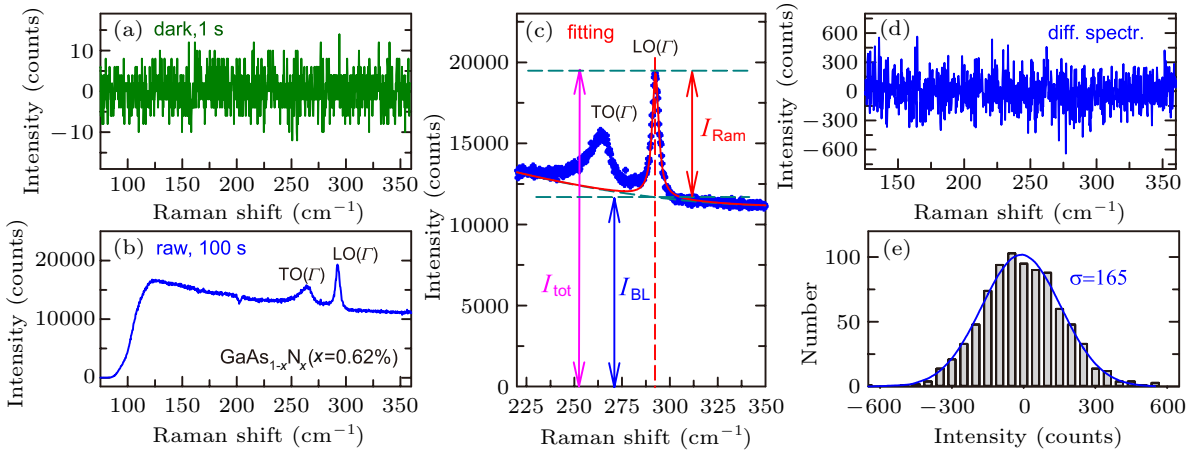

Fig. 11. (a) Dark spectrum detected by liquid-cooled Si CCD detector. The acquisition time is 1 second. The electronic offset is deducted before acquisition. (b) The raw Raman spectrum of $GaAs_{1-x}N_x$ ($x = 0.62\%$) under 671 nm excitation with acquisition time of 100 seconds. (c) Fitting of LO(Γ) peak for SNR analysis. The corresponding $I_{\rm Ram}$, $I_{\rm BL}$ and $I_{\rm tot}$ are marked. (d) The corresponding difference spectrum (diff.spectr.) between two successive measurements of (b). (e) The statistical distribution of the counts in (d) with $\sigma = 165$.

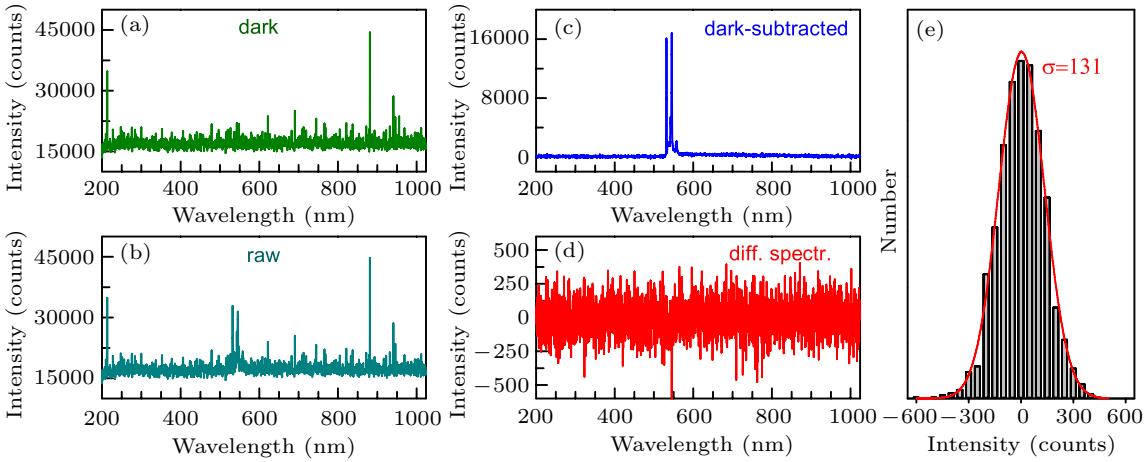

Fig. 12. (a) Dark spectrum detected by CCD detector working at 25 °C. (b) Raw Raman spectrum of BP. (c) The dark-subtracted Raman spectrum of BP. (d) The difference spectrum (diff.spectr.) between two successive dark-subtracted spectra. (e) The statistical distribution of count in (d) with $\sigma = 131$.

For multichannel detector with high Φ_d and non-uniformity in noise level and photoelectric response between different pixels, e.g., CCD detector working around room temperature and InGaAs array detector, the corresponding SNR analysis based on Eq. (17) can not be directly applied to the dark-subtracted spectrum whose electronic offset, background and non-uniformity of dark signal are together removed from the signal of interest. For example, for a CCD detector with a working temperature around room temperature, the measured dark spectrum is shown in Fig. 12(a). Raman signal from BP cannot be identified in the measured raw Raman spectrum in Fig. 12(b), which is overwhelmed by the non-uniformity of dark signals. However, the Raman signal can be clearly resolved in the dark-subtracted spectrum in Fig. 12(c). One can see that such subtraction is quite useful to yield S even the Raman features are overwhelmed by strong background. Raman software tends to directly display the dark-subtracted spectrum in the routine measurement. In this case, it is possible to perform SNR analysis on the measured Raman signal based on Eq. (16). It should be noted that this subtraction cannot remove the noise from the baseline, and average count of the baseline around Raman peaks is not directly related to σ_{BL}. If the baseline is almost constant around Raman peak of interest, the difference spectrum between two successive dark-subtracted spectra (Fig. 12(d)) can be used to estimate the noise of the baseline in the interested region, i.e., σ_{BL}, which is equal to the corresponding standard deviation (Fig. 12(e)) divided by $\sqrt{2}$. We obtain σ_{BL} of 92.6 for the strongest Raman signal of BP in Fig. 12(c). According to Eq. (16), the SNR of the strongest Raman peak of BP in Fig. 12(c) is about 102.

For all the measured Raman signals by multichannel detectors, the raw Raman data should be used in the SNR analysis without any artificial and technical smoothing by software or technician. Any such smoothing would lead to overestimation of the SNR for the measured Raman signal.

How to design and build a Raman spectroscopy system with high SNR has always been the concern of scientific instrument companies and researchers. The SNR analysis above provides guidance to instrumental design and routine measurement. Generally speaking, Raman spectrometer with negligible σ_r, σ_d and σ_B is recommended for measurement. When background is not a dominant source of noise, the simplest way to improve SNR is to improve the intensity of Raman signal by increasing the excitation power of laser or by extending the integration time of detector. Especially for LN_2-cooled or TE-cooled detectors with extremely low noise level, to minimize noise from external sources is a primary concern in instrumental design, such as securing all covers and closing all unused entrance or exit ports. With respective to rather weak signals requiring longer acquisition time, the dark noise then becomes the dominant issue, detectors with high quantum efficiency and low dark current are quite necessary.

7. Conclusion

To conclude, we introduce the recent advances on Raman spectroscopy of 2DMs, including N-dependent interlayer modes and Davydov splitting of intralayer modes in NL twisted $MoTe_2$. The relation between interlayer interactions and intralayer vibrations is directly established. We also overview various noise sources and their potential influences on SNR of Raman signals measured by CCD detectors and IGA array detector, which provides comprehensive strategies to reduce noise in Raman spectrum. This will be helpful to optimize SNR of Raman signal in instrument design and routine Raman measurements.

References

[1] Novoselov K S, Geim A K, Morozov S V, Jiang D, Zhang Y, Dubonos S V, Grigorieva I V and Firsov A A 2004 *Science* **306** 666
[2] Fiori G, Bonaccorso F, Iannaccone G, Palacios T, Neumaier D, Seabaugh A, Banerjee S K and Colombo L 2014 *Nat. Nanotechnol.* **9** 768
[3] Mounet N, Gibertini M, Schwaller P, Campi D, Merkys A, Marrazzo A, Sohier T, Castelli I E, Cepellotti A, Pizzi G and Marzari N 2018 *Nat. Nanotechnol.* **13** 246
[4] Li X L, Han W P, Wu J B, Qiao X F, Zhang J and Tan P H 2017 *Adv. Funct. Mater.* **29** 1604468
[5] Casiraghi C, Hartschuh A, Lidorikis E, Qian H, Harutyunyan H, Gokus T, Novoselov K S and Ferrari A C 2007 *Nano Lett.* **7** 2711
[6] Bruna M and Borini S 2009 *Appl. Phys. Lett.* **94** 031901
[7] Li Y L, Rao Y, Mak K F, You Y M, Wang S Y, Dean C R and Heinz T F 2013 *Nano Lett.* **13** 3329
[8] Seyler K L, Rivera P, Yu H Y, Wilson N P, Ray E L, Mandrus D G, Yan J Q, Yao W and Xu X D 2019 *Nature* **567** 66
[9] Zhang X, Han W P, Wu J B, Milana S, Lu Y, Li Q Q, Ferrari A C and Tan P H 2013 *Phys. Rev. B* **87** 115413
[10] Ferrari A C and Basko D M 2013 *Nat. Nanotech.* **8** 235
[11] Puretzky A A, Liang L B, Li X F, Xiao K, Wang K, Mahjouri-Samani M, Basile L, Idrobo J C, Sumpter B G, Meunier V and Geohegan D B 2015 *ACS Nano* **9** 6333
[12] Zhang X, Qiao X F, Shi W, Wu J B, Jiang D S and Tan P H 2015 *Chem. Soc. Rev.* **44** 2757
[13] Wu J B, Lin M L, Cong X, Liu H N and Tan P H 2018 *Chem. Soc. Rev.* **47** 1822
[14] Ferrari A C, Meyer J C, Scardaci V, Casiraghi C, Lazzeri M, Mauri F, Piscanec S, Jiang D, Novoselov K S, Roth S and Geim A K 2006 *Phys. Rev. Lett.* **97** 187401
[15] Zhao W J, Tan P H, Zhang J and Liu J 2010 *Phys. Rev. B* **82** 245423
[16] Cong C X, Yu T, Sato K, Shang J Z, Saito R, Dresselhaus G F and Dresselhaus M S 2011 *ACS Nano* **5** 8760
[17] Lee C, Yan H, Brus L E, Heinz T F, Hone J and Ryu S 2010 *ACS Nano* **4** 2695
[18] Luo X, Zhao Y Y, Zhang J, Xiong Q H and Quek S Y 2013 *Phys. Rev. B* **88** 075320
[19] Tan P H, Han W P, Zhao W J, Wu Z H, Chang K, Wang H, Wang Y F, Bonini N, Marzari N, Pugno N, Savini G, Lombardo A and Ferrari A C 2012 *Nat. Mater.* **11** 294
[20] Liang L B, Zhang J, Sumpter B G, Tan Q H, Tan P H and Meunier V 2017 *ACS Nano* **11** 11777
[21] Park H, Shin G H, Lee K J and Choi S Y 2020 *Nano Res.* **13** 576
[22] Debnath R, Maity I, Biswas R, Raghunathan V, Jain M and Ghosh A 2020 *Nanoscale* **12** 17272
[23] Chen C, Chen X L, Yu H Y, Shao Y C, Guo Q S, Deng B C, Lee S, Ma C, Watanabe K, Taniguchi T, Park J G, Huang S X, Yao W and Xia F N 2019 *ACS Nano* **13** 552
[24] Holler J, Meier S, Kempf M, Nagler P, Watanabe K, Taniguchi T, Korn T and Schuller C 2020 *Appl. Phys. Lett.* **117** 013104
[25] Lin M L, Tan Q H, Wu J B, Chen X S, Wang J H, Pan Y H, Zhang X, Cong X, Zhang J, Ji W, Hu P A, Liu K H and Tan P H 2018 *ACS Nano* **12** 8770

[26] Parzefall P, Holler J, Scheuck M, Beer A, Lin K Q, Peng B, Monserrat B, Nagler P, Kempf M, Korn T and Schuller C 2021 *2D Mater.* **8** 035030

[27] Lin M L, Zhou Y, Wu J B, Cong X, Liu X L, Zhang J, Li H, Yao W and Tan P H 2019 *Nat. Commun.* **10** 2419

[28] McCreery R L 2000 *Raman Spectroscopy for Chemical Analysis* (John Wiley& Sons, Inc.) pp. 49–61

[29] Chen S, Lin X Q, Yuen C, Padmanabhan S, Beuerman R W and Liu Q 2014 *Opt. Express* **22** 12102

[30] Kibria B M G and George F 2014 *Commun. Stat. Simul. Comput.* **43** 443

[31] Fan X G, Zeng Y J, Zhi Y L, Nie T, Xu Y J and Wang X 2021 *J. Raman Spectrosc.* **52** 890

[32] Schulze H G, Yu M M L, Addison C J, Blades M W and Turner R F B 2006 *Appl. Spectrosc.* **60** 820

[33] Barton S J, Ward T E and Hennelly B M 2018 *Anal. Methods* **10** 3759

[34] Tan P H 2018 *Raman Spectroscopy of two-dimensional materials* (Singapore: Springer)

[35] Novoselov K S, Geim A K, Morozov S V, Jiang D, Katsnelson M I, Grigorieva I V, Dubonos S V and Firsov A A 2005 *Nature* **438** 197

[36] Zhang X, Tan Q H, Wu J B, Shi W and Tan P H 2016 *Nanoscale* **8** 6435

[37] Cong X, Lin M L and Tan P H 2016 *J. Semicond.* **40** 091001

[38] Wu J B, Zhang X, Ijäs M, Han W P, Qiao X F, Li X L, Jiang D S, Ferrari A C and Tan P H 2014 *Nat. Commun.* **5** 5309

[39] Stenger I, Schue L, Boukhicha M, Berini B, Placais B, Loiseau A and Barjon J 2017 2*D Mater.* **4** 031003

[40] Yagmurcukardes M, Peeters F M and Sahin H 2018 *Phys. Rev. B* **98** 085431

[41] Lui C H, Ye Z P, Ji C, Chiu K C, Chou C T, Andersen T I, Means-Shively C, Anderson H, Wu J M, Kidd T, Lee Y H and He R 2015 *Phys. Rev. B* **91** 165403

[42] Huang S X, Liang L B, Ling X, Puretzky A A, Geohegan D B, Sumpter B G, Kong J, Meunier V and Dresselhaus M S 2016 *Nano Lett.* **16** 1435

[43] Leng Y C, Lin M L, Zhou Y, Wu J B, Meng D, Cong X, Li H and Tan P H 2021 *Nanoscale* **13** 9732

[44] Wu J B, Hu Z X, Zhang X, Han W P, Lu Y, Shi W, Qiao X F, Ijäs M, Milana S, Ji W, Ferrari A C and Tan P H 2015 *ACS Nano* **9** 7440

[45] Li H, Wu J B, Ran F R, Lin M L, Liu X L, Zhao Y Y, Lu X, Xiong Q H, Zhang J, Huang W, Zhang H and Tan P H 2017 *ACS Nano* **11** 11714

[46] Froehlicher G, Lorchat E, Fernique F, Joshi C, Molina-Sanchez A, Wirtz L and Berciaud S 2015 *Nano Lett.* **15** 6481

[47] Song Q J, Tan Q H, Zhang X, Wu J B, Sheng B W, Wan Y, Wang X Q, Dai L and Tan P H 2016 *Phys. Rev. B* **93** 115409

[48] Tan Q H, Zhang X, Luo X D, Zhang J and Tan P H 2017 *J. Semicond.* **38** 031006

[49] Na W, Kim K, Lee J U and Cheong H 2019 *2D Mater.* **6** 015004

[50] Chen H, Xu W L, Broderick N and Han J D 2018 *J. Raman Spectrosc.* **49** 1529

[51] Mu Z D, Zhao X W. Xie Z Y, Zhao Y J, Zhong Q F, Bo L and Gu Z Z 2013 *J. Mater. Chem. B* **1** 1607

[52] McCreery R L 2000 *Raman Spectroscopy for Chemical Analysis* (John Wiley& Sons, Inc.) p. 188

[53] Stchur P, Cleveland D, Zhou J and Michel R G 2002 *Appl. Spectrosc. Rev.* **37** 383

[54] Zong C, Xu M X, Xu L J, Wei T, Ma X, Zheng X S, Hu R and Ren B 2018 *Chem. Rev.* **118** 4946

[55] Liu W, Liu S L, Chen D N and Niu H B 2014 *Chin. Phys. B* **23** 104202

[56] Zonios G 2010 *Appl. Opt.* **49** 163

[57] Tan P H, Xu Z Y, Luo X D, Ge W K, Zhang Y, Mascarenhas A, Xin H P and Tu C W 2006 *Appl. Phys. Lett.* **89** 101912